applied sciences

MDPI

Article

Fault Current and Voltage Estimation for Pole-To-Pole Faults in Modular Multilevel Converter Based DC Grids Considering AC Active Power

Hui Cai [1], Junli Zhang [2], Jingqiu Yu [2] and Zheren Zhang [2,*]

[1] State Grid Jiangsu Electric Power Co. LTD., Economic Research Institute, Nanjing 210008, China; caihui300@hotmail.com
[2] Department of Electrical Engineering, Zhejiang University, Hangzhou 310058, China; 11910064@zju.edu.cn (J.Z.); yujingqiu@zju.edu.cn (J.Y.)
* Correspondence: zhangzheren@zju.edu.cn

Abstract: DC short-circuit faults are one of the challenges for modular multilevel converter (MMC) based DC grid. It is vital for proper design of protection system to estimate the fault currents and voltages. The existing calculation methods based on RLC equivalent model of MMC have enough accuracy in estimating the branch currents but suffer from poor accuracy in estimating the node voltages. To better reflect the dynamics of MMC control during the fault, MMC is equivalent to a RLC series circuit in parallel with a variable controlled current source. This model not only considers the discharge of sub-module capacitors but also the AC active power and MMC control. Then, based on the discrete adjoint model of the equivalent MMC model and the RL series equivalent model of DC lines, the fault voltages and currents for the pre-fault and faulted DC grids could be easily obtained. From the aspect of power balance, the importance of AC active power on estimating the fault currents and voltages is discussed then. At last, based on the Zhangbei bipolar DC grid, comparisons are conducted between the simulations on PSCAD, the numerical calculation under the proposed method and the existing methods. The results show that the proposed method and the existing methods are both able to accurately estimate the fault currents within a relative error of 1%. However, compared with the error of the existing methods in calculating the fault voltages, the relative error for the proposed method is limited to less than 5% for the whole DC gird.

Keywords: modular multilevel converter (MMC); DC grid; discrete adjoint model; fault current and voltage

Citation: Cai, H.; Zhang, J.; Yu, J.; Zhang, Z. Fault Current and Voltage Estimation for Pole-To-Pole Faults in Modular Multilevel Converter Based DC Grids Considering AC Active Power. *Appl. Sci.* **2021**, *11*, 2882. https://doi.org/10.3390/app11062882

Academic Editor: Paweł Szcześniak

Received: 01 March 2021
Accepted: 19 March 2021
Published: 23 March 2021

1. Introduction

High-voltage large-capacity flexible DC transmission, with its advantages of controllable trend, easy to absorb new energy, and ability to provide reactive power support, has become an important pillar of the future DC grid [1–4]. Among the various topologies, modular multi-level (MMC) converter is the preferred topology due to the advantages of high scalability and low harmonic [5].

The short-circuit fault is one of the critical contingencies for an AC/DC hybrid system. One of the shortcomings for the half-bridge sub-module structure is that it does not have the ability to clear DC faults, and it needs to be equipped with DC circuit breakers to isolate the fault line [6–8]. The fault current generated during this period is harmful and critical for the secure and safe operation of DC grid. For properly design of fault current limiting and fault blocking devices, an accurate calculation method of fault current and voltage is very necessary [9,10].

The traditional short-circuit transient characteristic calculation method for DC grid is electromagnetic transient (EMT) simulation [11–14]. However, this method suffers from

low efficiency and high computation burden. In [15], a generic calculation method for pole-to-pole short-circuit fault currents in DC grids is proposed. Based on the simplified RLC equivalent of MMC, it presents a simple numerical analysis. Literature on MMC modeling shows that the minimum required complexity for dynamic MMC modeling has to include the outer controllers and partial dynamics [16,17]. In [18], relying on the modified averaged value models, DC fault current simulation is performed for protection design in radial multi-terminal DC systems. In [19], the dynamic analysis is carried out for voltage source converter based multi-terminal DC grids (VSC-MTDC) in order to analytically design a generalized feedback for DC voltage droop control. Although, converter outages and communication loss are considered, the article does not analyze line outages or DC faults. To improve the efficiency of the calculation method, MMCs are equivalent to RLC series circuits and the phase-mode conversion method is adopted to simplify the model of the whole DC grid in [20]. However, when the DC grid is radial or mesh, there are some difficulties in performing this method. In [21], the effect of the AC side on the DC short-circuit current is considered, and it provides accurate estimation for short-circuit currents. However, since the influence of MMC control is not considered, there are still some errors in estimating the fault currents and fault voltages. In [22,23], the accuracy for all the node voltages and branch currents could be improved by the inclusion of MMC controllers. However, the equivalent current sources for converters in the active power control are treated as constant. However, the active and reactive power take changes very sharply especially several milliseconds after the pole-to-pole fault. Therefore, the assumption that the active power keeps constant during the fault leads to some bias especially in estimating the node voltages. Therefore, to guarantee enough accuracy, the dynamics of the AC active power should be involved.

This paper makes in-depth analyses of the AC active power on the transient characteristics. From the perspective of the power balance, it is proved that the deviation of AC power results in a relatively large error in calculating the node voltages. Fortunately, the real-time transmitted AC active power and the dynamics of the MMC controllers can be reflected through improving the model of MMC. Based on this, a MMC is equivalent to a RLC series circuit in parallel with a variable controlled current source. Next, the whole DC grid is discretized by the discrete adjoint model. By this method, the dynamics of the controllers can be easily included. At last, the formulas and solutions for the matrices describing the relationship between the branch currents and the node voltages are given. Thus, a general method for estimating the branch currents and node voltages is established.

The features and contributions of this paper are as the follows. (1) The influence of the AC active power on estimating the node voltages and branch currents is fully analyzed. The absence of the AC active power will lead a wrong conclusion that the DC voltage of the inverter station rises after the fault. The deviation of AC active power will lead to small bias in estimating node voltages. (2) Instead of adopting the constant equivalent current sources for converters in the active power control mode, variable current sources are used to model the control dynamics of MMCs in active power modes. The accuracy in estimating the node voltages could thus be improved.

The rest of this paper is organized as follows. Section 2 equivalents MMC to a RLC series model in parallel with a variable current source taking into account the MMC controllers and the AC active power. Section 3 establishes the equivalent model for the whole DC grid based on the discrete adjoint model. Section 4 gives the pre-fault and faulted matrices describing the node voltages and branch currents, and a general method for calculating the transient voltages and currents is proposed. Section 5 verifies the accuracy of the proposed method. Section VI draws the conclusions.

2. The Equivalent Model of MMC Considering AC Side Power and MMC Control

2.1. The Impact of AC Active Power and MMC Controllers

The basic structure of the MMC is illustrated in Figure 1. The converter consists of six arms, and the upper and lower arm in the same phase form a phase unit. Each arm consists of two parts, i.e., N series-connected identical sub-modules (SMs) and an arm inductor L_{arm}. The equivalent arm resistor and the SM capacitor are denoted as R_{arm} and C_0, respectively. The smoothing reactor is denoted as L_{dc}.

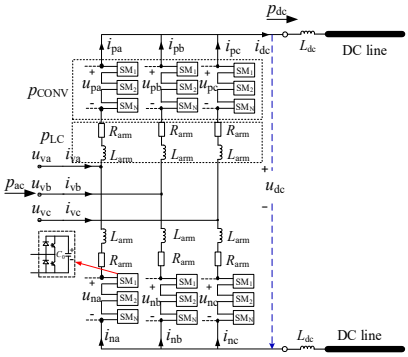

Figure 1. Basic structure of MMC.

Here in Figure 1, u_{rj} and i_{rj} are the arm voltage and the arm current, where j ($j = a, b, c$) denotes phase and r ($r = p, n$) denotes the upper or lower arm. i_{vj} is the MMC AC output current in phase j. u_{vj} is the AC voltage at the point of common coupling (PCC) in phase j. u_{dc} is the DC voltage, and i_{dc} is the DC current.

At any time instant, the instantaneous power p_{dc} at the DC terminal is the sum of the instantaneous AC active power at the AC terminal p_{ac}, the instantaneous powers resulting from the derivative of energy of the phase reactors p_L and the module capacitors p_{CONV}. Here, the phase reactor losses and converter losses are neglected. The relationship could then be described in Equation (1):

$$p_{dc} = p_{ac} + p + _{L_{CONV}} \quad (1)$$

From the above equation, accurately estimating the branch currents and node voltages requires the equivalent MMC model well to reflect the power balance in the transient excursion. p_{CONV} results from the variation in time of the controlled voltage, which is also the voltage across the module capacitor. In steady-state, this voltage is equal to the DC voltage at the terminal of the MMC. In transient excursion, the controlled DC voltage might be different from the terminal DC voltage due to the action of the controllers. Therefore, p_{CONV} has to be estimated differently based on DC control mode and the terminal DC voltage during the transient.

2.2. The Equivalent MMC Model Considering AC Active Power and MMC Controllers

In the generic RMS model, the equivalent MMC model is shown in Figure 2 [24]. The behavior of the MMC on the DC side is equal to a controlled current source i_s. The effect of p_{ac} is reflected by the controlled current source. The part of p_{CONV} estimated by the terminal DC voltage is reflected in the derivative of energy of the equivalent capacitance. Similarly, the power from the derivative of energy of the equivalent inductance and equivalent resistance is p_{LC}. The expression of the controlled current source, the equivalent capacitance, inductance and resistor is given in Equation (2).

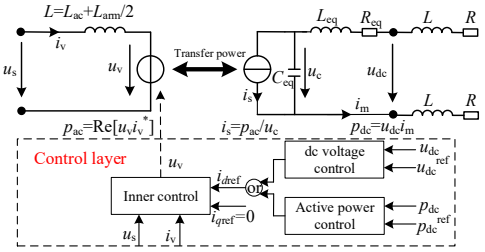

Figure 2. Equivalent model of MMC.

$$i_s = \frac{p_{\text{ac}}}{u_c},\ L_{\text{eq}} = \frac{2}{3}L_{\text{arm}},\ R_{\text{eq}} = \frac{2}{3}R_{\text{arm}},\ C_{\text{eq}} = \frac{6C_0}{N} \tag{2}$$

where p_{ac} is power transmitted from the AC side. u_{c} is the voltage across the equivalent capacitor.

However, the controlled DC voltage is absent in this model, that is, p_{CONV} related to the DC control mode is not involved. Since MMC controllers take effect during the fault, the control mode would affect the output voltage on the AC side of MMC and then the transient characteristics of the DC side. However, the control strategy of the DC side could be implemented via the controlled DC voltage as a constituent component of the controlled arm voltages. That is, taking into account the control mode in computing the output voltage u_{v}, the unaccounted power could be compensated by this improvement.

According to the nearest level modulation (NLM) strategy [25,26], MMC AC output voltage could be calculated as follows.

$$\begin{cases} u_{vj}(t) = \dfrac{m}{2}v_{con} * (t_0)\sin\left(\omega t + \varphi_j(t_0)\right) \\ \varphi_j(t_0) = arctan\dfrac{v^*_{q\text{ref}}(t_0)}{v^*_{d\text{ref}}(t_0)} \\ v_{dc\,con}(t_0) = \sqrt{{v^*_{d\text{ref}}}^2(t_0) + {v^*_{q\text{ref}}}^2(t_0)} \end{cases} \tag{3}$$

where, m is the modulation ratio of the converter. ω is the angular frequency of the AC side. $v_{d\text{ref}}^*$ and $v_{q\text{ref}}^*$ are the outputs of the inner loop current controller.φ_j is the phase difference between the MMC AC output voltage and the AC voltage in phase j. t_0 represents the last moment.

Then the power injected into the converter from the AC side could be computed as follows:

$$p_{ac} = \frac{3u_{s\,j}u_{v\,j}}{X_s + 0.5X_{arm}\sin\varphi_j} \tag{4}$$

From Equations (3) and (4) and Figure 2, it could be seen that the DC control mode affects the MMC AC output voltage and then the AC active power. In fact, the AC active power and MMC control influence the discharge of submodule capacitors and thus the DC transient voltages and currents, which could roughly be estimated as follows.

It is assumed there is an error Δp_{ac} in estimating the AC active power. Then the error in estimating the controlled current source would be $\Delta i_{\text{s}} = \Delta p_{\text{ac}}/u_{\text{c}}$. Here, it is assumed that the voltage of the capacitors is equal to the DC voltage terminal of the MMC. Then the error in node voltages would be

$$\Delta u_{dc} = \frac{u_c}{c_{ceq} \approx \frac{\Delta p_{ac}}{c_{dc_{eq}}}} \frac{\Delta i_s}{\Delta p_{ac}} \tag{5}$$

For a DC grid, C_{eq} is typically hundreds to thousands μF. u_{dc} is usually hundreds to thousands kV. Then an error of several hundred MW in p_{ac} would lead an error of several

dozen kV/ms in Δu_{dc}. In several ms after the fault, the error in fault voltages would be several dozen kV.

The error in estimating the branch currents could be evaluated from the deviation of line currents. Let u_1, u_2 and i_L be the voltages and current of the line, and then the error would be

$$\Delta \quad \frac{\frac{\Delta u_1 - \Delta u_2}{L}}{i_L} \tag{6}$$

The line inductance L is typically several hundreds to thousands mF. Taking into account the errors in fault voltages, the maximum estimation bias in Δi_L would be less than one kA/ms. Then in several ms after the fault, the maximum error in i_L would be about one kA.

In summary, by combining the control strategy with the controlled current source, the power balance is well expressed. And not only the branch currents but also the node voltages could be estimated accurately by the improved equivalent MMC model shown in Figure 2.

2.3. The Model of MMC Controllers

The control strategy of MMC is relatively mature. In this paper, the classic inner and outer loop control methods are used for calculation [4,27,28]. The specific control algorithm is not repeated in this article. All variables in Equations (7)–(9) are unit values. The positive direction of the AC currents is injecting into the converter.

For the station with constant power control, the instantaneous expression of the outer loop controller is:

$$\begin{cases} \Delta p^*(t) = P^*_{\text{ref}} - p^*(t) \\ i^*_{\text{kp}}(t) = k_{\text{pp}} \Delta p^*(t) \\ i^*_{\text{ki}}(t) = k_{\text{ip}} \left(\Delta p^*(t) + \Delta p^*(t_0) \right) \Delta t / 2 + i^*_{\text{ki}}(t_0) \\ i^*_{\text{dref}}(t) = i^*_{\text{kp}}(t) + i^*_{\text{ki}}(t) \\ i^*_{\text{qref}}(t) = 0 \end{cases} \tag{7}$$

For the station with constant voltage control, the instantaneous expression of the outer loop controller is:

$$\begin{cases} \Delta u^*_{\text{dc}}(t) = U^*_{\text{dcref}} - u^*_{\text{dc}}(t) \\ i^*_{\text{kp}}(t) = k_{\text{pu}} \Delta u^*_{\text{dc}}(t) \\ i^*_{\text{ki}}(t) = k_{\text{iu}} \left(\Delta u^*_{\text{dc}}(t) + \Delta u^*_{\text{dc}}(t_0) \right) \Delta t / 2 + i^*_{\text{ki}}(t_0) \\ i^*_{\text{dref}}(t) = i^*_{\text{kp}}(t) + i^*_{\text{ki}}(t) \\ i^*_{\text{qref}}(t) = 0 \end{cases} \tag{8}$$

where, k_{pp}, k_{ip} and k_{pu}, k_{iu} are proportional and integral coefficient of constant power controller and constant voltage controller, respectively. u_{dcref}^* is the reference value of DC voltage. p_{ref}^* is the reference value of active power. p^* is the instantaneous value of active power. i_{dref}^* is the reference current of d-axis, i_{qref}^* is the reference current of q-axis.

The expression of the inner loop controller is:

$$\begin{cases} \Delta i_d^*(t) = i_{dref}^{**d} \\ \Delta i_q^*(t) = i_{qref}^{**q} \\ \Delta v_{dkp}^{*=p2_d^*} \\ \Delta v_{dki} \\ *_{i2}\left(\Delta i_d^*(t) + \Delta i_d^*(t_0)\right)/_{dki}^{*0} \\ \Delta v_{qkp}^{*=p2_q^*} \\ \\ \\ \\ \\ \\ \Delta v_{qki}^{*i2\left(\Delta i_q^*(t)+\Delta i_q^*(t_0)\right)/_{qki_v}^{*0}} \end{cases} \begin{matrix} \\ \\ \\ \\ \\ \\ {}^{**d}_{*qki} \\ {}^{*q}_{qkp} \\ v_{qref} \\ dkp \\ {}^{**q}_{*dki} \\ {}^{dref}_{*d} \end{matrix} \quad (9)$$

where, k_{p2} and k_{u2} are the proportional and integral coefficients of the inner loop controller. i_d^* and i_q^* are the d-axis and q-axis of the AC current. u_d^* and u_q^* are the d-axis and q-axis of the AC voltage u_s.

3. Discrete Adjoint Model of DC Grid

The characteristic of discrete adjoint model is that the lumped parameter element is converted into a parallel connection of an admittance and a current source according to the state of its history voltage and current. Thus, a circuit network originally described by differential-algebraic equations could be transformed into a network that could only be described by algebraic equations [4].

The discrete adjoint model of the series-connected resistor-inductor branch is shown in Figure 3, and the corresponding voltage and current characteristics are listed in Equation (10).

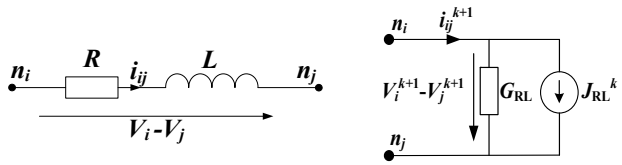

Figure 3. Discrete adjoint model of series-connected resistance-inductor branch: (a) original circuit; (b) discrete adjoint model.

$$\begin{cases} i_{ij}^{k+1} = G_{\mathrm{RL}}\left(V_i^{k+1} - V_j^{k+1}\right) + J_{\mathrm{RL}}^k \\ G_{\mathrm{RL}} = h/(L + hR) \\ J_{\mathrm{RL}}^k = L i_{ij}^k/(L + hR) \end{cases} \quad (10)$$

where, h is the time step. L is the inductance of the branch; R is the resistance of the branch. The superscript k indicates the current step, and the superscript $(k + 1)$ indicates the next step. i is the branch current. V is the node voltage. G_{RL} is the equivalent admittance, and J_{RL} is the equivalent current source.

The discrete adjoint model of the capacitor branch is shown in Figure 4, and the corresponding voltage and current characteristics are shown in Equation (11).

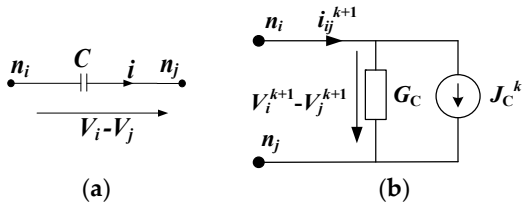

Figure 4. Discrete adjoint model of capacitor branch: (**a**) original circuit; (**b**) discrete adjoint model.

$$\begin{cases} i_{ij}^{k+1} = G_C\left(V_i^{k+1} - V_j^{k+1}\right) + J_C^k \\ G_C = C/h \\ J_C^k = -C\left(V_i^k - V_j^k\right)/h \end{cases} \tag{11}$$

where, G_C is the equivalent admittance and J_C is the equivalent current source. The other variables have been defined as above.

By replacing the MMC equivalent circuit with the discrete adjoint model of the basic components, the discrete adjoint model of an MMC could be obtained, as shown in Figure 5.

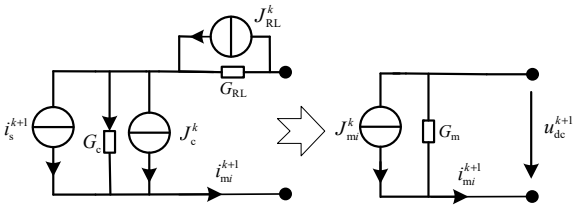

Figure 5. Discrete adjoint model of MMC.

Combing Equations (10) and (11) with the KVL and KCL laws:

$$\begin{aligned} i_{mi}^{k+1} &= G_{mi} u_{dc}^{k+1} + J_{mi}^n \\ G_{mi} &= 1 \Big/ \left(\frac{L_{eq}}{h} + R_{eq} + \frac{h}{C_{eq}} \right) \\ J_{mi}^n &= \left(u_c^n - \frac{L_{eq}}{h} i_{dc}^n - \frac{h}{C_{eq}} i_s^{n+1} \right) \Big/ \left(\frac{L_{eq}}{h} + R_{eq} + \frac{h}{C_{eq}} \right) \end{aligned} \tag{12}$$

In a large-scale DC grid, the overhead transmission lines are used to deliver bulk power over a long distance. The DC overhead lines are represented as a RL series circuit. The smoothing reactor on both sides of the MMC could be involved into the equivalent model of the lines. As shown in Figure 2, *R* represents the equivalent resistance of the DC line and *L* represents the DC reactor.

All MMC converters can be equivalent to RLC series circuits parallel with the controlled current sources, and DC lines can be equivalent to RL series circuits. On this basis, it is easy to obtain the discrete adjoint model of the DC grid.

4. Short-Circuit Characteristic Calculation Method

4.1. Node Voltage Equations for the Pre-Fault DC Grid

In order to describe the calculation method more clearly, the nodes and branches need to be defined firstly. It is assumed that the DC grid has 2*n* nodes (*n* nodes in the positive pole and *n* nodes in the negative pole) and *b* branches. The nodes of the positive pole and negative pole are denoted as n_i and n_{i+n} (i = 1,2…n), respectively. The reference direction for the branch currents of the lines is defined as the direction from node n_i to n_j.

DC line from node n_i to node n_j is denoted as l_{ij}. The numbering subscript in the voltage, the current, the equivalent admittance and the equivalent current source in a specific branch is in accordance with the numbering subscript of the branch.

The MMC bus nodes are defined as the real nodes, and the line connection nodes are defined as the virtual nodes. It is assumed that there is an MMC between the corresponding virtual nodes of the positive pole and the negative pole, and the admittance G_m of the virtual MMC are set to be zero.

According to the defined positive directions of currents and voltages, the simplified model between any two adjacent nodes of the positive pole and the negative pole is shown in Figure 6.

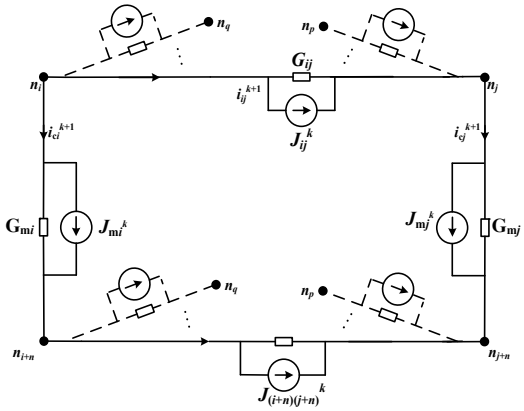

Figure 6. Simplified model between any two adjacent nodes.

For node n_i and n_j, the node voltage equations could be derived as follows:

$$\begin{aligned}\left(G_{mi}+\sum_{q\in i}G_{iq}\right)V_i^{k+1}-G_{mi}V_{i+n}^{k+1}-\sum_{q\in i}G_{iq}\,V_q^{k+1}&=-J_{mi}^{k}-\sum_{q\in i}J_{iq}^{k}\\ \left(G_{mj}+\sum_{p\in j}G_{pj}\right)V_j^{k+1}-G_{mj}V_{j+n}^{k+1}-\sum_{p\in j}G_{pj}\,V_p^{k+1}&=-J_{mj}^{k}+\sum_{p\in j}J_{pj}^{k}\end{aligned}\tag{13}$$

For node n_{i+n} and n_{j+n}, the node voltage equations could be derived as follows:

$$\begin{aligned}\left(G_{mi}+\sum_{q+n\in i+n}G_{(i+n)(q+n)}\right)V_{i+n}^{k+1}-G_{mi}V_i^{k+1}-\sum_{q+n\in i+n}G_{(i+n)(q+n)}\,V_{q+n}^{k+1}&\\ =J_{mi}^{k}-\sum_{q+n\in i+n}J_{(i+n)(q+n)}^{k}&\\ \left(G_{mj}+\sum_{p+n\in j+n}G_{(p+n)(j+n)}\right)V_{j+n}^{k+1}-G_{mj}V_j^{k+1}-\sum_{p+n\in j+n}G_{(p+n)(j+n)}\,V_{p+n}^{k+1}&\\ =J_{mj}^{k}+\sum_{p+n\in j+n}J_{(p+n)(j+n)}^{k}&\end{aligned}\tag{14}$$

Here, V means the node voltage. The symbol $\in$ means that the two nodes are connected to each other. G_{ij} and J_{ij} are the equivalent admittance and the equivalent current source of line l_{ij}. The other symbols have been defined above.

The node voltage matrix $\boldsymbol{V}_0$, the equivalent current source matrix $\boldsymbol{J}_0$ of the DC lines, and $\boldsymbol{J}_c$ of the MMCs are defined as Equations (15)–(17). It is assumed that the rows from 1 to n of these matrices correspond to the equivalent current source of the nodes in the positive pole, and the rows from $n + 1$ to the end correspond to the equivalent current source of the nodes in the negative pole.

$$V_0 = [V_1\ V_2\ \cdots\ V_{n+1}\ \cdots\ V_{2n}]_{2n}^T \tag{15}$$

$$J_0 = \left[J_{12}\ \cdots\ J_{ij}\ \cdots J_{(n+1)(n+2)}\ \cdots\ J_{(i+n)(j+n)}\ \cdots\right]_b^T \tag{16}$$

$$J_c = [-J_{c1}\ \cdots -J_{cn}\ J_{c\,1}\ \cdots\ J_{cn}\ ]_{2n}^T \tag{17}$$

Thus, the relationship between the node voltages and the equivalent current sources can be obtained in Equation (18).

$$G_0 \bullet V_0 = J_c - A_0 \bullet J_0 \tag{18}$$

Here in Equation (18), $\mathbf{A_0}$ is the pre-fault correlation matrix between the nodes and the branches, and its dimension is $2n \times b$. $\boldsymbol{G_0}$ is the pre-fault admittance matrix, and its dimension is $2n \times 2n$.

According to the reference direction of the current defined as above, the elements in $\mathbf{A_0}$ can be defined in Equation (19).

$$a_{ij} = \begin{cases} 1 & (\text{node } i \text{ is the starting point of the branch } l_{ij}) \\ -1 & (\text{node } i \text{ is the terminal point of the branch } l_{ij}) \\ 0 & (\text{node } i \text{ is not a point of the branch}) \end{cases} \tag{19}$$

The elements in $\boldsymbol{G_0}$ are defined as follows:

(1) Diagonal elements: The diagonal elements in $\boldsymbol{G_0}$ are the sum of admittances on branches directly connected to nodes, that is

$$G_{ii} = G_{mi} + \sum_{j \in i} G_{ij} \tag{20}$$

(2) Non-diagonal elements: The meaning of the non-diagonal elements is the negative value of the admittances of the branches directly connected to the two nodes.

According to the above method, it is easy to establish the nodal voltage equations in the form of matrix for the pre-fault DC grid, which is suitable for any grid structure. For the faulted DC grid, the branch current matrix, current source matrix and admittance matrix could be modified accordingly to the fault.

4.2. Modification of the Matrices for the Fault DC Grid

It is assumed that a pole-to-pole fault occurs between line l_{ij} and line $l_{(i+n)(j+n)}$. The fault point is denoted as n_f at line l_{ij} and n_{f+n} at line $l_{(i+n)(j+n)}$. Node n_{f+n} could be set as the reference node, and its reference voltage could be treated as $-u_{dc}/2$. Thus, the voltage of node n_f is $u_{dc}/2$. Therefore, for pole-to-pole fault, the number of the unknown node voltages do not increase. However, branch l_{ij} and branch $l_{(i+n)(j+n)}$ are replaced by branch l_{if}, l_{fj} and branch $l_{(i+n)(f+n)}$, $l_{(f+n)(j+n)}$. Since the node voltages V_f and V_{f+n} are treated as known, adding the pole-to-pole fault means the branches l_{ij} and line $l_{(i+n)(j+n)}$ no longer exist, while the origin nodes are connected to the known nodes. Therefore, the dimension of these matrices remains the same, and the elements are very easy to modify.

The elements in $\boldsymbol{J_0}$ and $\boldsymbol{J_c}$ should be modified as:

$$\begin{cases} J_{ij}^{'} = 0 \\ J_{(i+n)(f+n)}^{'} = 0 \\ J_{c\,i}^{'} = J_{c\,i} + G_{if}V_f - J_{if} \\ J_{c(i+n)}^{'} = J_{c(i+n)} + G_{(i+n)(f+n)}V_{(f+n)} - J_{(i+n)(f+n)} \\ J_{c\,j}^{'} = J_{c\,j} + G_{fj}V_f + J_{fj} \\ J_{c(j+n)}^{'} = J_{c(j+n)} + G_{(f+n(j+n))}V_{(f+n)} + J_{(f+n)(j+n)} \end{cases} \tag{21}$$

The correlation matrix $\mathbf{A_0}$ remains the same, but the admittance matrix $\boldsymbol{G_0}$ need to be modified. Since there are no new nodes, only the self-admittances of node n_i and n_j should be modified and the mutual admittance between node n_i and n_j should be eliminated.

$$\begin{cases} \boldsymbol{G_0'(i,j) = G_0'(j,i) = 0} \\ \boldsymbol{G_0'(i+n,j+n) = G_0'(j+n,i+n) = 0} \\ \boldsymbol{G_0'(i,i) = G_0(i,i) + G_{if}} \\ \boldsymbol{G_0'(i+n,i+n) = G_0(i+n,i+n) + G_{(i+n)(f+n)}} \\ \boldsymbol{G_0'(j,j) = G_0(j,j) + G_{fj}} \\ \boldsymbol{G_0'(j+n,j+n) = G_0(j+n,j+n) + G_{(f+n)(j+n)}} \end{cases} \tag{22}$$

5. Case Study

5.1. Description of the Test System

The test system adopted in this paper is the Zhangbei ±500 kV four-terminal bipolar DC grid in china. Its schematic diagram is illustrated in Figure 7. Kangbao, Zhangbei, Fengning and Beijing converter stations are abbreviated as s_1-s_4. Parameters of the Zhangbei DC grid are listed in Table 1. Generally, due to the delay of the communication system, the converters receive the blocking signal and then execute the blocking command with a delay of several cycles. Considering the factors such as short-term DC withstand voltage and thermal stress tolerance, the delay should generally not exceed 10 ms. This paper is suitable for estimating the fault characteristics prior to the blocking, but unfortunately the blocking of MMCs cannot be modeled. Therefore, an identical calculation step of 10 ms and time step of 50 us is set for the EMT simulation performed on PSCAD and the presented method performed on MATLAB.

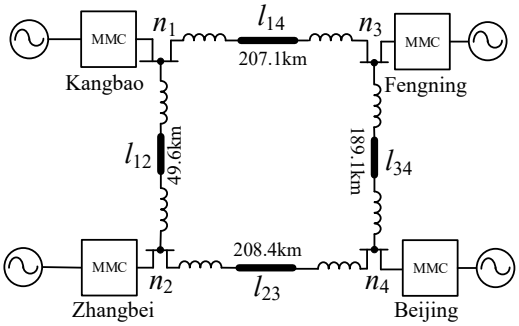

Figure 7. Schematic Diagram of the Zhangbei ±500 kV bipolar DC grid.

Table 1. Main Circuit Parameters of the Test System.

Items	Values
Converter Stations	
Rated AC voltage (kV)	230 (s_1,s_3)/525 (s_2,s_4)
Transformer impedance(p.u.)	0.0176 (s_1,s_3)/0.0088 (s_2,s_4)
Smoothing reactor(mH)	300
Rated capacity(MW)	1500 (s_1,s_3)/3000 (s_2,s_4)
Rated DC voltage	±500 kV
Arm inductor(mH)	40 (s_1,s_3)/75 (s_2,s_4)
SM capacitor(uF)	10000 (s_1,s_3)/15000 (s_2,s_4)
Number of SMs per arm	218
DC transmission lines	
Resistance per unit length	0.009735 Ω/km
Inductance per unit length	0.0176 mH/km

Capacitance per unit length	0.001367 μF/ km
Control mode	
S_1	Q = 0 MVar, P = −1500 MW
S_2	Q = 0 MVar, P = −3000 MW
S_3	Q = 0 MVar, P = 1500 MW
S_4	Q = 0 MVar, U_{dc} = ±500 kV

5.2. Influence of the AC Infeed

Taking into account the AC infeed during the fault, the energy is well balanced between the AC side and the DC side:

$$E_{\mathrm{dc}} = E_{\mathrm{ac}} + EL_{CONV} \tag{23}$$

where, E_{dc} represents the energy storage of DC side including the energy in lines and reactors. E_{ac} represents the energy input from the AC system, and E_{CONV} represents the released energy of an MMC converter. E_L is the released energy of the phase reactors. E_{dc} and E_{ac} can be calculated as follows:

$$\begin{aligned} E_{\mathrm{dc}} &= \int_{t_0}^{t_0+\Delta t} p_{\mathrm{dc}} dt \\ E_{\mathrm{ac}} &= \int_{t_0}^{t_0+\Delta t} p_{\mathrm{ac}} dt \end{aligned} \tag{24}$$

where, t_0 is when the fault occurs. $\triangle t$ is the calculation time.

Since the equivalent resistance of the arm is usually small, the energy change of the resistance can be ignored. The energy storage components of the MMC mainly include the sub-module (SM) capacitors. The total stored energy of the SM capacitors and the inductors are respectively listed as follows.

$$E\frac{1}{2}\sum_{j=a,b,c}\frac{2C_0}{N}\left(\left(u_{pj}^2(t_0+\Delta t)-u_{pj}^2(t_0)\right)+\left(u_{lj}^2(t_0+\Delta t)-u_{lj}^2(t_0)\right)\right)_{CON} \tag{25}$$

$$E=\frac{L_{\mathrm{arm}}}{2}\left(\sum_{j=a,b,c}\left(i_{pj}^2(t_0+\Delta t)-i_{pj}^2(t_0)\right)+\sum_{j=a,b,c}\left(i_{lj}^2(t_0+\Delta t)-i_{lj}^2(t_0)\right)\right)_L + \frac{L_{dc}}{2\left(i_{dc}^{2(t_0+\Delta t)}{}_{dc}^{2(t_0)}\times 2\right)} \tag{26}$$

According to the analysis of power transfer among the AC side, DC side and MMC's internal components, the influence of the AC active power on the fault currents and voltages could be studied. Based on Equations (23)–(26), the energy changes of the DC side, MMC internal components and AC side of each converter station within 10 ms after the fault occurs with and without AC infeed are shown in Figure 8.

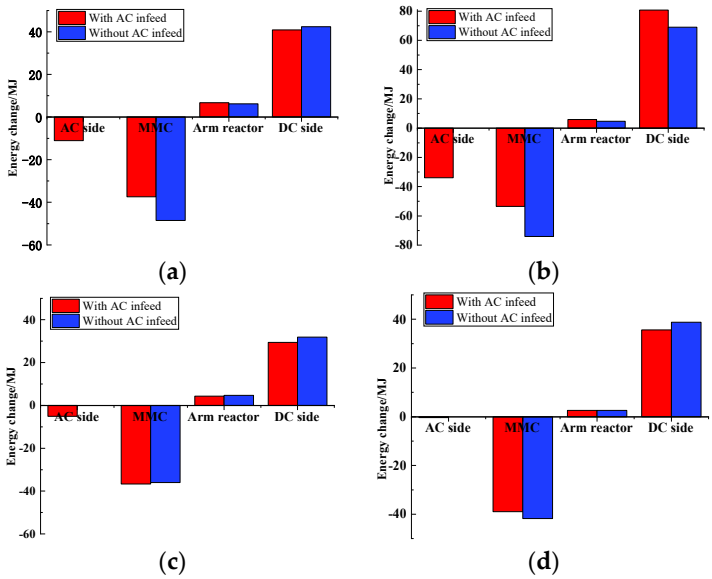

Figure 8. Energy changes between the AC side and DC side: (**a**) station s_1; (**b**) station s_2; (**c**) station s_3; (**d**) station s_4.

It could be seen from Figure 8 that whether the AC infeed is taken into account or not, the energy of the SM capacitors changes the most. For sending end converter stations (such as s_1 and s_2), the energy released by the SM capacitors is reduced when there is AC infeed. For receiving end converter stations (such as s_3 and s_4), the energy released by the SM capacitors increases when the AC side absorbs energy from the DC system. As a dynamic energy balance between the AC side and the SMs is maintained in the whole process, the energy released to the DC side changes slightly.

For station s_1 and s_2, AC active power can make up part of the power required by the DC side, delaying the discharge rate of the sub-module capacitors. For station s_3 and s_4, there is a rise in the energy of the SMs capacitor for a short period of time without AC infeed. Due to the freewheeling effect of the smoothing reactor, the pre-fault current injecting into the converter will not be reversed immediately. When the AC active power is taken into the calculation, the DC current flowing into the converter station is absorbed by the AC system. When the DC current is reversed, the AC side and the DC side release energy together. Therefore, the total energy of AC system changes very small. And the DC voltage of the MMC drops slower than the response speed of the controller. In this case, the modulation ratio drops very fast, leading to a dynamic imbalance between the modulation ratio and the DC voltage. At this stage, MMC is in a state of undermodulation, which makes the average SM capacitor voltage rises passively and the energy of the capacitor increases. Therefore, accurately estimating the branch currents and node voltages needs considering the AC side power and MMC control.

5.3. Accuracy Validation of the Proposed Method

To show the importance of the AC side power on estimating the branch currents and node voltages, here is a comparison of the results with and without AC infeed. It is assumed that the system has already been in steady-state. At t = 0 ms, a pole-to-pole fault occurs on the line side of s_1 at line l_{12}. Table 2 gives the initial values of branch currents and node voltages. Figures 9 and 10 show the comparison between the current results and the voltage results obtained by numerical calculation and EMT simulation, respectively.

Table 2. Steady-state Values of the Pole-to-pole Voltage and Branch Current.

Item	i_{10}/kA	i_{20}/kA	i_{13}/kA	I_{24}/kA	I_{34}/kA
Value	−0.694	0.694	1.434	2.210	0.682
Item	u_{dc1}/kV	u_{dc2}/kV	u_{dc3}/kV	u_{dc4}/kV	/
Value	1008.72	1009.86	1002.39	1000.00	/

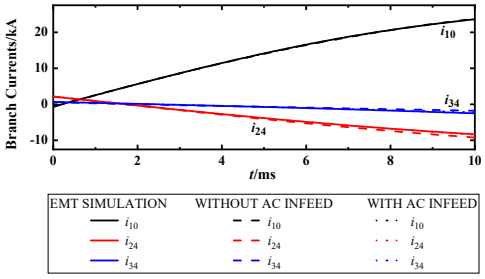

Figure 9. Branch currents obtained by EMT simulation and numerical calculation.

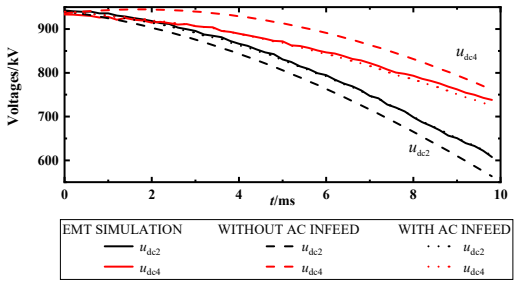

Figure 10. DC voltages at the terminal of S_2 and S_4 obtained by EMT simulation and numerical calculation.

It could be seen from Figure 9 that the branch currents coincide with those computed by the EMT simulation. This is achieved by including the MMC control into the AC output voltage of MMC. The proposed method also shows good accuracy in the unfaulted branch currents i_{24} and i_{34} especially at 5−10 ms after the fault since the controller takes effect at this time.

From Figure 10, it could be seen that there are evident errors in estimating node voltages if AC infeed is not considered. For sending end converter station S_2, the voltage u_{dc2} decreases much faster than the proposed method. For receiving end converter station S_4, the voltage u_{dc4} firstly rises to some extent and then decreases. This is because the AC side releases the power required by the DC side for the sending end and plays the role of absorbing and releasing power flowing into the converter station for the receiving end. Since all MMC controllers are represented by variable controlled current sources, the proposed method shows sufficient accuracy in estimating the node voltages.

5.4. Accuracy Enhancement of the Presented Method

The methods proposed in [22,23] are endowed with greatly improved accuracy since the impacts of MMC control are involved. However, the equivalent DC current sources for converters in the active power control mode are assumed to be constant, leading to small bias in estimating the node voltages. Different from them, a variable current source is adopted in this paper to model the control dynamics of MMCs in active power and voltage control modes. The improved accuracy in estimating the node voltages will be expressed as follows.

5.4.1. Pole-To-Pole Fault Near Station s_1 under Constant Active Power Control

It is assumed that the system has already been in steady-state. At t = 0 ms, a pole-to-pole fault occurs on the line side of s_1 at line l_{12}. The results obtained by the simulations, the proposed method and the methods in [22,23] are shown in Figure 11. The relative errors are also given in Figure 11. It could be seen that compared with the results obtained by the method in [22,23], the proposed method shows improved accuracy in estimating the node voltages. Especially, for stations s_1 and s_3 with large AC active power change during 5–10 ms after the fault, the proposed method shows tiny errors in estimating the node voltages. Since the control dynamics are taken into account, the errors in estimating the node voltages can be reduced to less than 5%. It could also be seen from Figure 11e that the proposed method and the method in [22,23] estimate the branch currents accurately in about the same extent.

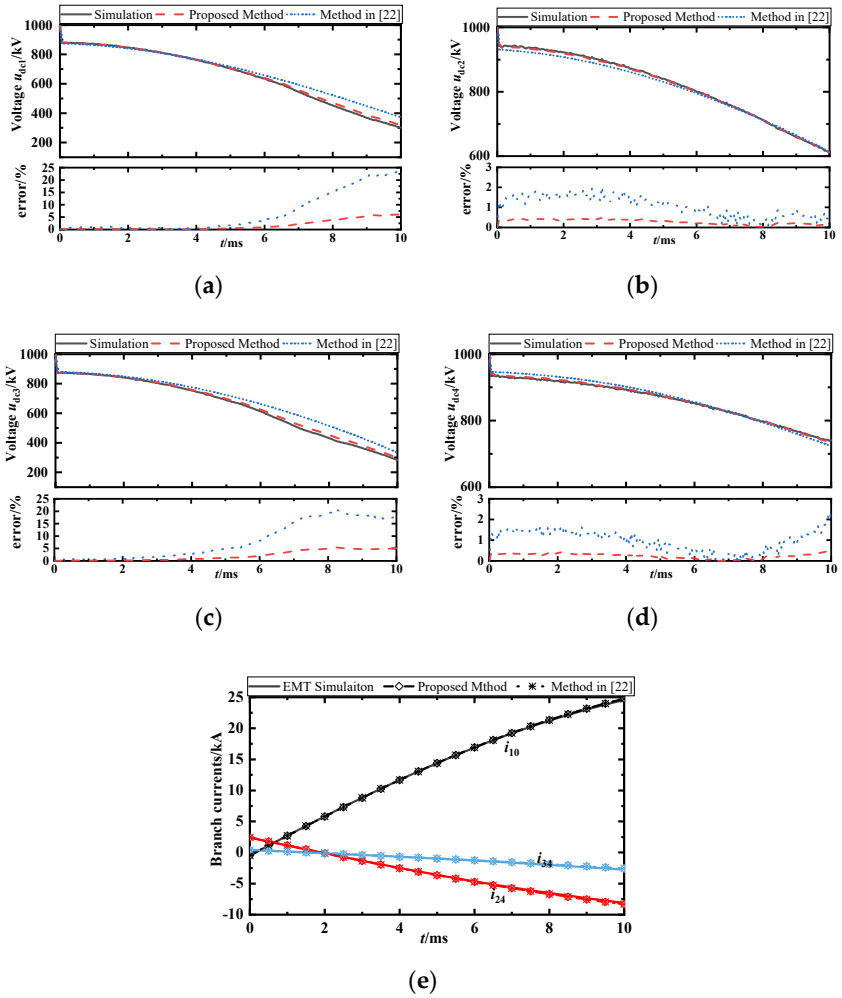

Figure 11. Branch currents and node voltages obtained by EMT simulation, the proposed method and the method in [22]: (**a**) u_{dc1} of station s_1; (**b**) u_{dc2} of station s_2; (**c**) u_{dc3} of station s_3; (**d**) u_{dc4} of station s_4; (**e**) branch currents.

5.4.2. Pole-To-Pole Fault Near Station s_4 under Constant DC Voltage Control

It is assumed that the system has already been in steady-state. At t = 0 ms, a pole-to-pole fault occurs on the line side of s_4 at line l_{24}. The results and errors obtained by simulations, the proposed method and the methods in [22,23] are shown in Figure 12.

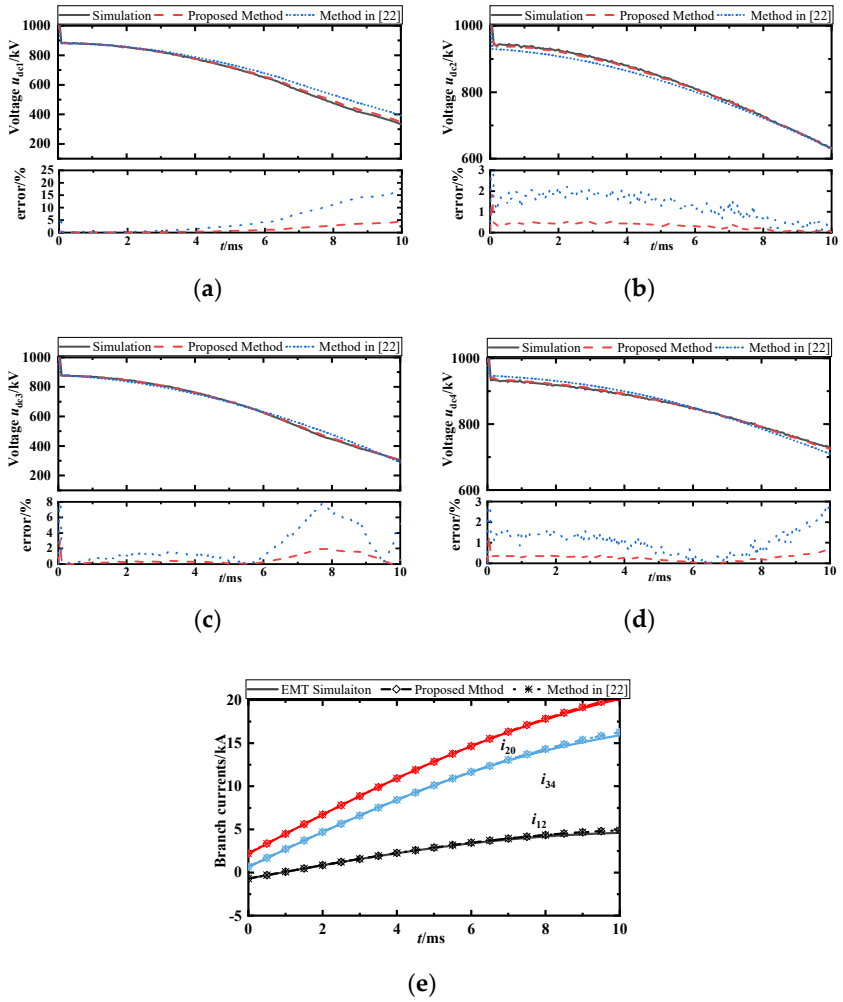

Figure 12. Branch currents and node voltages obtained by EMT simulation, the proposed method and the method in [22]: (**a**) u_{dc1} of station s_1; (**b**) u_{dc2} of station s_2; (**c**) u_{dc3} of station s_3; (**d**) u_{dc4} of station s_4; (**e**) branch currents.

Similar conclusions could be drawn from Figure 12 that the proposed method shows greatly improved accuracy in estimating the node voltages especially 5–10 ms after the fault. The branch currents could be estimated accurately in both the proposed method and the method in [22,23].

In summary, it could be concluded from Sections 5.3 and 5.4 that high accuracy shows in the branch currents and node voltages computed by the presented method and EMT simulation no matter where the fault occurs. Compared with the existing methods, the proposed method gives more accurate node voltages of the whole DC grid.

6. Conclusions

From the perspective of power balance, this paper proposes a highly accurate estimation method of the fault currents and fault voltages for the whole bipolar DC grid. The following conclusions could be drawn from the comparisons between the EMT simulation and numerical calculation.

(1) For the sending end converter, the active power on the AC side slows down the discharge rate of the sub-module capacitors. For the receiving end converter, the AC side plays the role of absorbing and releasing energy. Therefore, AC active power are supposed to be taken into account in the equivalent DC model of MMC.

(2) By modeling all MMC controls and AC active power as variable controlled current sources, compared with the existing literature, the accuracy for estimating the node voltages is greatly improved, especially for converters with large active power change during the fault. Besides, the relative errors in the node voltages are all reduced to less than 5%, which shows the sufficient accuracy of the proposed method.

(3) High accuracy is guaranteed by the propose method in estimating the branch currents and node voltages in the stage of capacitor discharging after the fault. Unfortunately, the converter blocking phase cannot be modelled with this method. How the proposed method could be used for dealing with the transient characteristics estimation during the freewheeling stage and steady state after the fault will be further discussed in the future work.

Author Contributions: Data curation, J.Z.; Formal analysis, H.C. and J.Y.; Investigation, J.Z.; Methodology, Z.Z.; Project administration, H.C.; Software, J.Y.; Supervision, J.Y.; Validation, Z.Z.; Visualization, J.Z. and Z.Z.; Writing—original draft, H.C. and J.Z.; Writing—review & editing, J.Y. and Z.Z. All authors have read and agreed to the published version of the manuscript.

Funding: This research received no external funding.

I**nstitutional Review Board Statement:** Not Applicable.

Informed Consent Statement: Not Applicable.

Data Availability Statement: Not Applicable.

Conflicts of Interest: The authors declare no conflict of interest.

References

1. Nami, A.; Liang, J.; Dijkhuizen, F.; Demetriades, G.D. Modular multilevel converters for HVDC applications: Review on converter cells and functionalities. *IEEE Trans. Power Electron.* **2015**, *30*, 18–36.
2. Zhao, B.; Song, Q.; Li, J.; Xu, X.; Liu, W. Comparative analysis of multilevel-high-frequency-link and multilevel-DC-link DC-DC transformers based on MMC and dual-active-bridge for MVDC application. *IEEE Trans. Power Electron.* **2018**, *33*, 2035–2049.
3. Tang, Y.; Chen, M.; Ran, L. A compact MMC submodule structure with reduced capacitor size using the stacked switched capacitor architecture. *IEEE Trans. Power Electron.* **2016**, *31*, 6920–6936.
4. Xu, Z. *Modular Multilevel Converter-Based High Voltage DC Power Transmission Systems*, 2nd ed.; China Machine Press: Beijing, China, 2016; pp. 378–380.
5. Bucher, M.K.; Wiget, R.; Andersson, G.; Frank, M.C. Multiterminal HVDC networks—What is the preferred topology? *IEEE Trans. Power Del.* **2014**, *29*, 406–413.
6. Liu, G.; Xu, F.; Xu, Z.; Zhang, Z.; Tang, G. Assembly HVDC breaker for HVDC grids with modular multilevel converters. *IEEE Trans. Power Electron.* **2017**, *32*, 931–941.
7. Mokhberdoran, A.; Hertem, D.V.; Silva, N.; Leite, H.; Carvalho, A. Multi-port hybrid HVDC circuit breaker. *IEEE Trans. Ind. Electron.* **2017**, *65*, 309–320.
8. Shukla, A.; Demetriades, G. A survey on hybrid circuit-breaker topolo-gies. *IEEE Trans. Power Del*. **2015**, *30*, 627–641.
9. Shi, J.; Tang, Y.; Chen, L. The application of active superconducting DC fault current limiter in hybrid AC/DC power supply systems. *IEEE Trans. Appl. Supercond.* **2008**, *18*, 672–675.
10. Li, C.; Gole, A.M.; Zhao, C. A fast dc fault detection method using dc reactor voltages in HVDC grids. *IEEE Trans. Power Del.* **2018**, *33*, 2254–2264.
11. Bucher, M.K.; Franck, C.M. Contribution of fault current sources in multi-terminal HVDC cable networks. *IEEE Trans. Power Del.* **2013**, *28*, 1796–1803.
12. Han, X.; Sima, W.; Yang, M.; Li, L.; Yuan, T.; Si, Y. Transient characteristics under ground and short-circuit faults in a ±500 kV MMC-based HVDC system with hybrid dc circuit breakers. *IEEE Trans. Power Del.* **2018**, *33*, 1378–1387.
13. Zhang, Z.; Xu, Z. Short-circuit current calculation and performance requirement of HVDC breakers for MMC-MTDC systems. *IEEE Trans. Electr. Electron. Eng.* **2016**, *11*, 168–177.
14. Tünnerhoff, P.; Ruffing, P.; Schnettler, A. Comprehensive fault type discrimination concept for bipolar full-bridge-based MMC HVDC sys-tems with dedicated metallic return. *IEEE Trans. Power Del.* **2018**, *33*, 330–339.
15. Li, C.; Zhao, C.; Xu, J.; Ji, Y.; Zhang, F. An A pole-to-pole short circuit fault current calculation method for dc grids. *IEEE Trans. Power Syst.* **2017**, *32*, 4943–4953.
16. Liu, S.; Xu, Z.; Hua, W.; Tang, G.; Xue, Y. Electromechanical transient modeling of modular multilevel converter based multi-terminal HVDC systems. *IEEE Trans. Power Syst.* **2014**, *29*, 72–83.
17. Li, Y.; Tang, G.; Ge, J.; He, Z.; Pang, H.; Yang, J.; Wu, Y. Modeling and damping control of modular multilevel converter based dc grid. *IEEE Trans. Power Syst*. **2018**, *33*, 723–735.

18. Li, R.; Xu, L.; Holliday, D.; Page, F.; Finney, S.J.; Williams, B.W. Continuous operation of radial multiterminal HVDC systems under dc fault. *IEEE Trans. Power Del.* **2016**, *31*, 351–361.
19. Eriksson, R. Current sharing in multi-terminal dc grids—The analytical approach. *IEEE Trans. Power Syst.* **2018**, *33*, 6278–6288.
20. Tang, L.; Dong, X. An approximate method for the calculation of transmission line fault current in MMC-HVDC grid. *Proc. CSEE* **2019**, *39*, 178–186.
21. Duan, G.; Wang, Y.; Yin, T.; Yin, S.; Li, G.; Sun, S. DC short circuit current calculation for modular multilevel converter. *Power Syst. Technol.* **2018**, *42*, 2145–2152.
22. Langwasser, M.; Carne, G.D.; Liserre, M.; Biskoping, M. Fault current estimation in multi-terminal HVdc grids considering MMC control. *IEEE Trans. Power Syst.* **2019**, *34*, 2179–2189.
23. Langwasser, M.; de Carne, G.; Biskoping, M.L.M. Improved fault current calculation method for pole-to-pole faults in MMC Multi-Terminal HVDC Grids Considering Control Dynamics. In Proceedings of the 2018 IEEE Energy Conversion Congress and Exposition (ECCE), Portland, OR, USA, 23–27 September 2018; pp. 5529–5535.
24. Trinh, N.; Zeller, M.; Wuerflinger, K.; Erlich, I. Generic Model of MMC-VSC-HVDC for interaction study with AC power system. *IEEE Trans. Power Syst.* **2016**, *31*, 27–34.
25. Wang, J.; Bai, H.M.Z. A submodule fault ride-through strategy for modular multilevel converters with nearest level modulation. *IEEE Trans. Power Electron.* **2018**, *33*, 1597–1608.
26. Shen, K.; Wang, S.; Zhao, D.; Zhao, G. A discrete-time low-frequency-ratio nearest level modulation strategy for modular multilevel converters with small number of power modules. *IEEE Access* **2019**, *7*, 25792–25803.
27. Liang, Y.; Liu, J.; Zhang, T.; Yang, Q. Arm current control strategy for MMC-HVDC under unbalanced conditions. *IEEE Trans. Power Del.* **2017**, *32*, 125–134.
28. Li, S.; Wang, X.; Yao, Z.; Li, T.; Peng, Z. Circulating current suppressing strategy for MMC-HVDC based on nonideal proportional resonant controllers under unbalanced grid conditions. *IEEE Trans. Power Electron.* **2015**, *30*, 387–397.